Solution of Inverse Problems in Thermal Systems

Yogesh Jaluria[1]
Mechanical Engineering Department,
Rutgers University,
Piscataway, NJ 08854
e-mail: jaluria@jove.rutgers.edu

A common occurrence in many practical systems is that the desired result is known or given, but the conditions needed for achieving this result are not known. This situation leads to inverse problems*, which are of particular interest in thermal processes. For instance, the temperature cycle to which a component must be subjected in order to obtain desired characteristics in a manufacturing system, such as heat treatment or plastic thermoforming, is prescribed. However, the necessary boundary and initial conditions are not known and must be determined by solving the inverse problem. Similarly, an inverse solution may be needed to complete a given physical problem by determining the unknown boundary conditions. Solutions thus obtained are not unique and optimization is generally needed to obtain results within a small region of uncertainty. This review paper discusses several inverse problems that arise in a variety of practical processes and presents some of the approaches that may be used to solve them and obtain acceptable and realistic results. Optimization methods that may be used for reducing the error are presented. A few examples are given to illustrate the applicability of these methods and the challenges that must be addressed in solving inverse problems. These examples include the heat treatment process, unknown wall temperature distribution in a furnace, and transport in a plume or jet involving the determination of the strength and location of the heat source by employing a few selected data points downstream. Optimization of the positioning of the data points is used to minimize the number of samples needed for accurate predictions.*
[DOI: 10.1115/1.4042353]

Keywords: inverse problems, unique solutions, uncertainty, practical systems, optimization

Introduction

Thermal systems and processes are of considerable interest in a wide variety of important engineering applications, ranging from energy and environment to transportation, heating, cooling, and manufacturing. In most problems, the boundary and initial conditions are well defined and the governing equations may be solved by analytical or numerical means to obtain the resulting flow, pressure, and temperature distributions from which heat transfer rates may be determined. This is the *forward* or *direct* problem and the literature has extensive results from direct solutions of many different problems of basic or applied interest. However, in many practical situations, the boundary conditions may not be accurately known or defined and the experimental determination of the relevant boundary conditions may be prohibitive in terms of cost and effort.

One such circumstance in which the boundary conditions are not known is the optical fiber drawing furnace in which a specially fabricated cylindrical glass rod known as a preform is heated and drawn into a fiber, as shown in Fig. 1(*a*). The temperature distribution at the furnace wall is a critical input to the simulation of the process. Figure 1(*b*) shows finite zones for calculating radiative heat transfer within the glass, which is an absorbing and emitting medium. Substantial work has been done on the optical fiber drawing process and accurate information on the wall temperature distribution has been shown to be essential for an accurate modeling [1,2]. Unfortunately, this distribution is not easily obtained experimentally because of high temperatures and limited access to the furnace. Modeling of the entire system is complicated by the presence of many control and traverse subsystems in the draw furnace. An *inverse* calculation using the limited temperature data obtained at certain locations may then be employed to determine the wall temperature distribution that gives rise to these data. However, such an inverse calculation generally does not yield unique results and strategies are needed to reduce the uncertainty in the results obtained [3–5].

Similarly, in several thermal processes, the desired result or output is known, but the conditions needed for achieving this output are to be determined. This circumstance again leads to an inverse problem. An example of this is the annealing heat treatment process shown in Fig. 2(*a*), where the thermal cycle needed to obtain desired product characteristics is known. The material, such as steel, is heated to its recrystallization temperature where the microstructure becomes pliable, held at this temperature for a duration known as soaking period to allow homogeneity in the piece and then cooled very slowly to a temperature below which the microstructure settles down in its new configuration [6]. An envelope indicating the acceptable deviation from the given thermal cycle for achieving the desired results is also shown. But the time-dependent heat input and temperatures are not known and need to be determined by solving the inverse problem. Figure 2(*b*) shows a sketch of a batch steel annealing furnace which is used for annealing steel sheets rolled into coils [7]. More is said on this furnace later. Annealing is used for materials like metals and alloys, as well as for glass and ceramics. Other processes, such as plastic thermoforming, have similar considerations and require an inverse solution to obtain the transport rates and temperatures that would lead to the desired temperature variation without violating given constraints. The inverse solution is then used to design the appropriate thermal system.

Another situation is one that often arises in thermal and material discharges into air and water environments. Frequently, the location of the source, as well as its strength or discharge rate, is not known. In such cases, measurements in the flow downstream of the jet or heat source may be used to obtain the source location and strength by solving the corresponding inverse problem. Here, the downstream temperature, concentration, and velocity data are known, but the source is not.

Despite the importance of inverse solutions in completing a given problem or for determining the conditions needed to achieve desired

[1]Corresponding author.

Contributed by the Heat Transfer Division of ASME for publication in the Journal of Thermal Science and Engineering Applications. Manuscript received October 3, 2018; final manuscript received December 7, 2018; published online June 6, 2019. Assoc. Editor: Ziad Saghir.

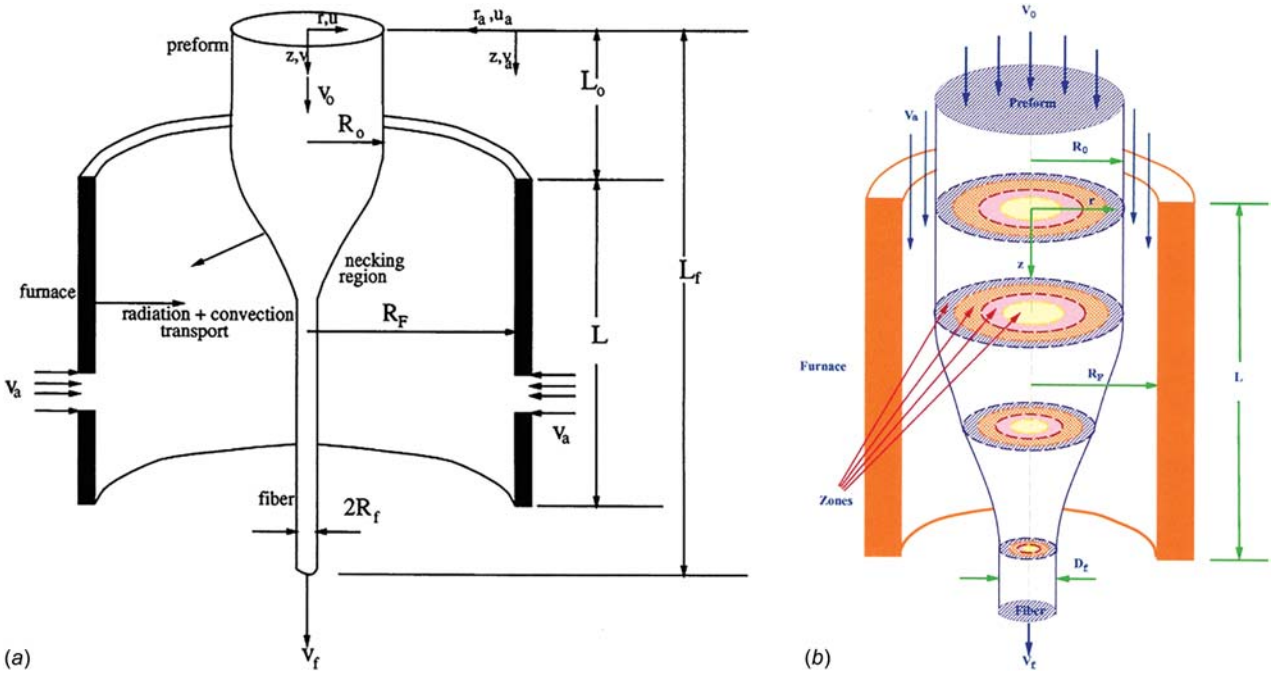

Fig. 1 (*a*) Furnace for optical fiber drawing, indicating the important transport mechanisms and (*b*) finite zones in the preform and fiber for the calculation of radiative heat transfer in the glass

results or for locating a thermal source or jet discharge that gives rise to a given flow, most of the work in the literature is devoted to the forward solutions and only a few studies to inverse problems. Inverse solutions in conduction heat transfer problems are more extensive than those in problems that involve convection or radiation due to nonlinear equations that arise in the latter set of problems. This paper considers the solution of inverse problems that arise in several practical situations and those that involve fluid flow, convection, and radiation. Thus, the direct solutions would generally involve nonlinearity, making both the direct and inverse solutions more involved. The narrowing of the region of uncertainty is also fairly complicated. This paper discusses some of the strategies that may be adopted to obtain the solution to such inverse problems with a fairly small region of uncertainty by using optimization techniques. The focus is on the inverse solution and the details on obtaining the forward solution, as well as the associated experimentation, are not given, leaving these to the references mentioned.

Analysis

The solution of an inverse problem typically starts by solving the direct problem at differing parametric values. The model is validated by comparing the results obtained with experimental data and analytical or numerical results in the literature. It is important to establish the validity and accuracy of the results from the model, including ensuring grid independence. These results are then considered in terms of the inputs and inverse interpolation functions are obtained. These functions are employed to obtain estimates of the missing boundary conditions. Obviously, this could lead to a range of possible solutions and a unique solution is generally not obtained. In order to narrow the domain in which the desired parameter or boundary condition lies, optimization techniques are employed. Optimization is also used to minimize the number of samples or data points needed for accurate predictions [8,9]. The optimization process is expected to reduce the uncertainty and ultimately lead to an essentially unique solution of the inverse problem.

The basic equations that are used to model the flow and thermal transport in thermal systems are based on the conservation of mass and energy and the force-momentum balance that give rise to the well-known Navier–Stokes equations for fluid flow and the energy equation for heat transfer. These may be written for a general three-dimensional process as [10]

$$\frac{\partial \rho}{\partial t} + \nabla \cdot (\rho \bar{V}) = 0 \tag{1}$$

$$\rho\left(\frac{\partial \bar{V}}{\partial t} + \bar{V} \cdot \nabla \bar{V}\right) = \bar{F} - \nabla p + \nabla \cdot \left[\mu\left(\nabla \bar{V} + \nabla \bar{V}^T\right)\right] - \frac{2}{3}\nabla(\mu \nabla \cdot \bar{V}) \tag{2}$$

$$\rho C_p\left(\frac{\partial T}{\partial t} + \bar{V} \cdot \nabla T\right) = \nabla \cdot (k \nabla T) + \dot{Q} + \mu\Phi + \beta T\left(\frac{\partial p}{\partial t} + \bar{V} \cdot \nabla p\right) \tag{3}$$

where ρ is the density, T is the temperature, t is the time, $\bar{V}$ is the velocity vector, $\bar{F}$ is the body force, p is the pressure, μ is the dynamic viscosity, C_p is the specific heat at constant pressure, β is the coefficient of volumetric thermal expansion, $\mu\Phi$ is the viscous dissipation, and $\dot{Q}$ is a volumetric heat source. The viscous dissipation and pressure work effects are included in the energy equation, Eq. (3), with the last two terms multiplied by βT representing the pressure effect. The bulk viscosity is taken as zero, giving the second viscosity coefficient λ as –(2/3) μ and Stokes' relationships are used for the viscous forces in the momentum equation, Eq. (2).

These equations can be used to obtain the applicable equations for thermal transport in a furnace, laminar natural convection induced by a finite heat source over a vertical or horizontal wall, forced convection from a heat source in a channel flow, and other thermal processes and systems. A turbulence model is required for turbulent flows, which are of interest in many practical processes such as flow induced by a fire and for buoyant jets in cross-flow. Radiative heat transfer in, for instance, glass for optical fiber drawing gives rise to a source term, which may be determined by methods such as the zonal method, using zones as shown in Fig. 1(*b*). A wide range of numerical methods are available to

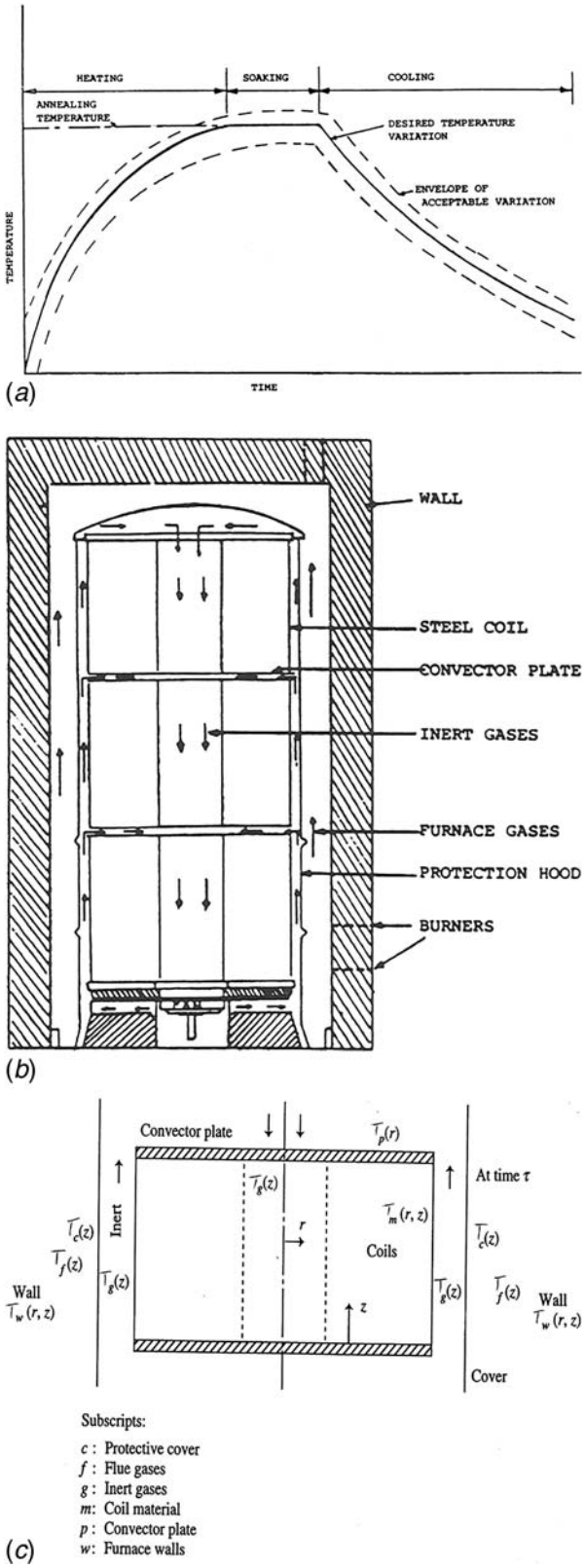

Fig. 2 (*a*) Temperature variation needed for an annealing process, (*b*) a batch annealing furnace for steel, and (*c*) modeling of some components of the furnace

solve these equations for different geometries and conditions. References given in this paper may be used to obtain details on the numerical methods that may be used as well as typical results obtained on these transport processes. The interpolation functions may be adopted to predict the desired conditions or inputs. These are then corrected using additional data points or an optimization process. Response surfaces and search methods may be used to narrow the domain in which the solution lies.

Results and Discussion

Several examples are given here to illustrate the use of the forward solution, along with optimization, to solve the relevant inverse problem.

Heat Treatment Furnace. An example of a heat treatment system was shown in Fig. 2(*b*), which gives a sketch of a batch annealing furnace for steel sheets rolled up into cylindrical coils [7,11,12]. The material has to be heated beyond its recrystallization temperature of around 723 °C and then cooled very slowly to achieve the desired annealing process, which removes residual stresses and restores ductility. Figure 2(*a*) shows, qualitatively, the desired temperature cycle, which involves slow cooling in the furnace. A faster cooling, with the furnace top removed, is often undertaken after reaching the temperature by which the grain structure is settled and annealing is complete. The boundary conditions, particularly the time-dependent flow of flue gases from the blast furnace, which provides the heat input into the furnace, need to be determined to obtain the desired temperature variation with time in the coils. Basic metallurgical considerations with respect to the heat treatment process are considered in deciding the specified temperature cycle.

This problem has to be numerically modeled and simulated to obtain the dependence of the temperature distributions on the boundary conditions. Different components, or subsystems, of the furnace are first modeled and then coupled to obtain the model for the entire system, as outlined in Refs. [7,13]. Figure 2(*c*) illustrates this process by showing some of the major components of this practical batch-annealing furnace for steel sheets. In the coiled steel sheets, the thermal conductivity k_r in the radial direction is often much smaller than k_z in the axial direction, due to gaps within the coils, and the governing conduction equation may be written taking this effect into account. Simplifications are made wherever possible. For instance, the thin cover, or protective hood, and the convector plate may be assumed to have uniform temperature across the thickness, the walls may be treated as one-dimensional transient cases, and the gases may be taken as well mixed, all these assumptions being based on scale analysis and governing parameters. Some of these approximations are indicated in Fig. 2(*c*). All the transport mechanisms, radiation, convection, and conduction, are considered, as appropriate, to yield conjugate problems, which are simulated numerically.

Once the simulation of the system is achieved, experimental validation is undertaken to ensure that the results obtained are valid and accurate. Figure 3(*a*) shows typical comparisons between the numerical and experimental results, indicating fairly good agreement and the accuracy of the numerical predictions. Additional results are given in Ref. [7]. Thus, the numerical simulation results may be employed for the design and optimization of the process as well as of the system. The results obtained from the simulation provide the necessary inputs for improving the existing designs, developing new designs, improving productivity, and improving the product quality for this manufacturing process. For instance, the dimensions and materials may be varied to reduce costs and improve the product, these changes being based on a thorough numerical simulation. For soaking, different control strategies may be considered, such as on/off systems, and simulated to choose an appropriate approach.

The heat treatment furnace is controlled by means of a temperature sensor located at the base of the furnace and in contact with the bottom surface of the lowest steel coil. The temperatures measured by this sensor are used to control the flow rate of the hot gases in order to achieve the desired annealing process. Using the simulation

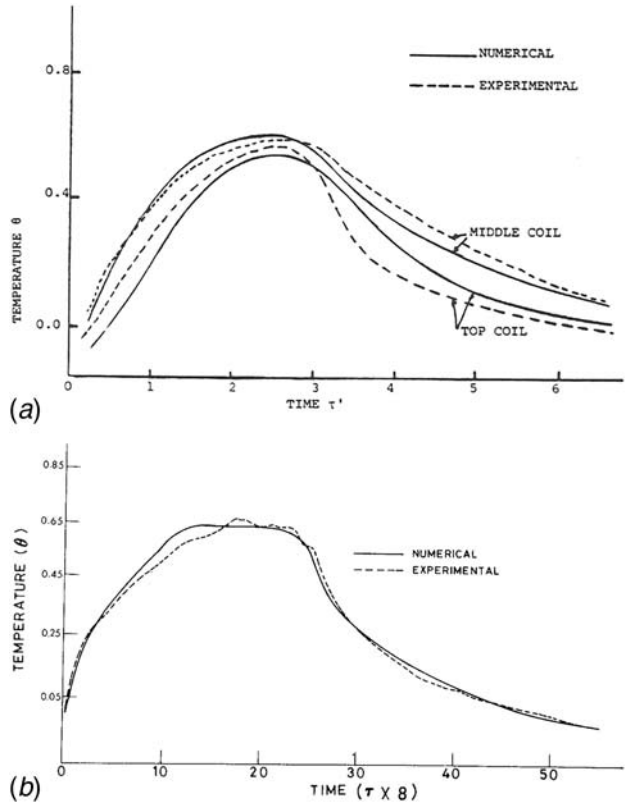

Fig. 3 (*a*) Comparison between numerical and experimental results on temperatures in the steel coils and (*b*) comparison between the inverse solution and experimental data on the control sensor temperature

results, the desired temperature variation at the sensor to achieve the given thermal cycle is determined by solving the resulting inverse problem. Interpolation functions and search methods for optimization are used. The interpolation functions are typically power-law, exponentials and polynomials, depending on the characteristics of the results obtained from the direct solution. These may be given as the following functions or combinations of these, depending on the results:

$$y_i = a\,x_i^n;\quad y_i = A\exp(-ax_i);$$
$$y_i = a_0 + a_1 x_i + a_2 x_i^2 + a_3 x_i^3 + \cdots + a_n x_i^n \tag{4}$$

where y_i represents the input parameter to be determined and x_i the known or given data. The a's are constants obtained from interpolation and curve fitting methods. Typically, linear and up to third-order polynomials are needed in most cases. Some examples are given later. The objective function Z is given in terms of the resulting error or uncertainty, an example of this being as

$$Z = \sum_{i=1}^{m}\left(\frac{y_{i,p} - y_{i,e}}{y_{i,e}}\right)^2 \tag{5}$$

where $y_{i,p}$ is the predicted value of the parameter to be determined and $y_{i,e}$ the actual or exact value of this parameter; m is the number of points in a continuous distribution considered for the inverse solution.

For the furnace, the input to be determined is the time-dependent sensor temperature, which controls the gas flow rate, and the known data are the temperatures in the steel coils, taken at a few selected points. Figure 3(*b*) shows a comparison between the numerical predictions and the experimental measurements from the control sensor. A fairly good agreement is observed, lending support to the model and the solution of the inverse problem to determine the boundary conditions needed to achieve the given thermal process. Similar processes are used for the annealing of parts made of glass, ceramics, aluminum, and other materials.

Fiber Draw Furnace Wall Temperature. A study of the flow and thermal transport associated with the optical fiber draw furnace requires accurate knowledge of the furnace wall temperature distribution. Even though an average, uniform, temperature has been used in many of the results in the literature, the dependence on the wall temperature distribution has also been investigated by a few investigators [14–16]. However, the wall temperature distribution is often not known. Due to high temperatures, furnace geometry, and inaccessibility, it is not possible to use sensors on the walls. Generally, a single temperature sensor is used for controlling the temperature of the wall and can be used to provide the value at a specific location. However, for accurate modeling of the process, the actual temperature distribution must be specified.

An experimental procedure involving mounting rods of different materials and diameters and feeding them axially within the furnace cavity was employed for this purpose by Issa et al. [17]. Figure 4(*a*) shows a typical fiber drawing furnace with a centrally located graphite rod. Each rod was instrumented with thermocouples inserted through an axial hole along the centerline. The temperature measurements were used along with the numerical model for the flow and heat transfer in the furnace in order to obtain the furnace wall temperature profile. This is an inverse problem since the centerline temperature in the rod is known, whereas the furnace thermal conditions are not known. The results obtained using graphite rods of different diameters indicated that the furnace temperature was not significantly affected by rod size, see Fig. 4(*b*). The temperatures at a few points on the graphite rod were taken as the known data and the wall temperature distribution is the input boundary condition to be determined by the inverse solution. The objective function was similar to that given in Eq. (5).

The measured temperature distribution along the axis of a graphite rod is shown, along with the wall temperature distribution obtained from the solution of the inverse problem. The dashed lines represent the water cooled portion of the furnace cavity. An optimization procedure based on *Lagrange multipliers* [13] is used to narrow the uncertainty in the non-unique solutions and obtain an essentially unique wall temperature distribution. This distribution is used to calculate the graphite rod temperature and a good agreement with the experimental data is observed. The computed maximum element temperatures were also in good agreement with the furnace sensor temperature at the hot zone centerline, as shown in Fig. 4(*c*), lending support to the model for the flow and thermal transport in the furnace and to the inverse solution. The small difference between the computed element temperatures for the two rod sizes is in support of the previous statement that there was a small influence of rod size on the furnace temperature distribution. Similar results were obtained for other furnace temperatures and for other materials, including silica glass.

Jets in Cross Flow. As mentioned earlier, in many engineering applications involving fluid-thermal systems, limited access to the flow domain is available and strong constraints are thus placed on the experimental data that can be obtained through techniques such as thermocouples and laser and infrared diagnostics. An important example of such limited access is a buoyant jet injected into a cross-flow. This flow is of interest in environmental problems due to thermal and material discharges into the environment. It will be useful to determine the location and strength of the discharge by measuring temperature or concentration downstream. Let us consider a two-dimensional jet being discharged perpendicular to a free stream flow, as shown in Fig. 5. The inflow is defined by the specified free stream conditions of velocity U_∞ and temperature T_∞. The jet is defined by the jet average velocity U_j and temperature T_j. The computational domain is shown. For the simulations, the

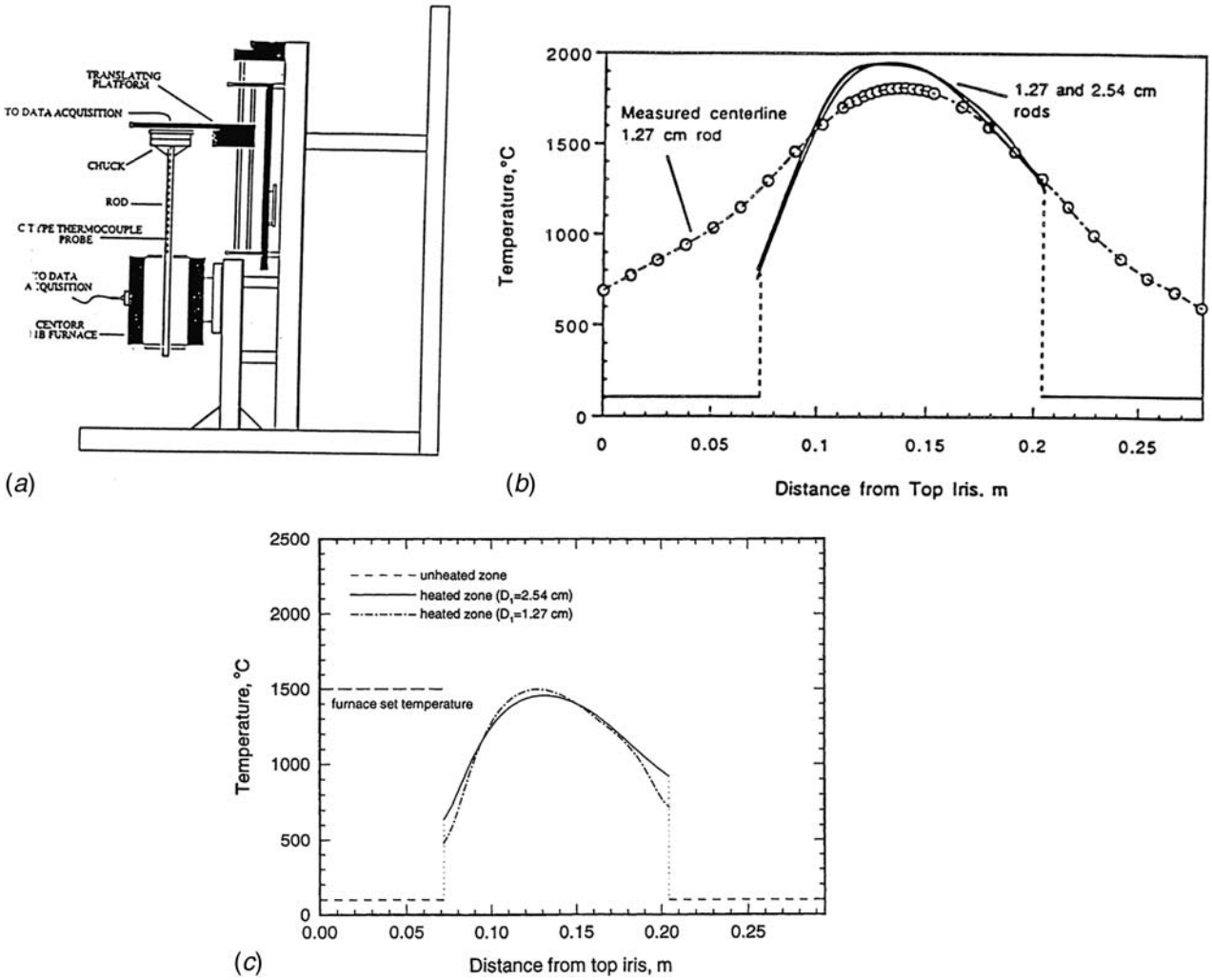

Fig. 4 (*a*) Schematic of an experimental system for measuring the temperature distribution in a rod located axially in an optical fiber drawing furnace and (*b*) computed furnace wall temperature distributions (solid line) from graphite rod data. Experimental points are for a 1.27 cm diameter rod. (c) Resulting furnace wall temperature distribution from the inverse solution and the measured furnace wall control sensor temperature.

free stream conditions are assumed to be known. By analogy to the optical fiber furnace, the jet average velocity U_j and temperature T_j are assumed to be unknown. Then, the objective is the determination of the jet average velocity U_j and temperature T_j based upon experimental data obtained downstream. In many cases, the access is limited, and in others, it is important to keep the data points at a minimum to reduce costs.

The experiments were performed in a low speed wind tunnel, with a test section of 0.7 m × 0.7 m in cross section and a length of 2 m. The maximum velocity in the test section is 30 m/s and is measured using a traversing pitot tube and wall pressure taps. The wind tunnel velocity is controlled using LabView. A two-dimensional slot jet protrudes from a flat plate with the jet centerline at a distance of 188 mm from the leading edge of the plate, see Fig. 6. The flat plate has a sharp leading edge and is raised above the wind tunnel floor to avoid the tunnel floor boundary layer. Pressurized air at 80 psia is split by a manifold into three separate flows that are separately metered by a standard rotameter. Each of the three independent flows is passed through two 700 W cartridge heaters (Omega AHP-7561). The maximum achievable temperature is 470 K at a flow rate of 25 scfm. The three flows are recombined in a settling chamber whose cross section is 50 mm × 610 mm. The jet flow is conditioned by two screens and a honeycomb section and flows in a constant area duct. A subsonic contraction accelerates the jet to the injection point. The jet has a parabolic velocity profile at injection. Each element of the jet injection system is insulated after the point of heat addition to minimize thermal losses. The jet exit temperature was measured by a small bead thermocouple at the jet exit and was observed to vary less than 2% across the jet exit.

A diode laser system is used to measure the time-varying absorbance across the flow field in the spanwise direction at selected locations from which the local temperature is obtained. A thermocouple is also used as a check on the measurements. Additional details are presented by Ma et al. [18]. A validation study was performed to assess the accuracy of the simulations by comparison with experiment. The difference between the computed and measured mean temperature was found to vary from 0.2% to 10.5%.

The experimental data were then used to determine the unknown jet velocity U_j and jet temperature difference $\Delta T_j = T_j - T_\infty$, using a third-order polynomial interpolation function, as given by Eq. (4). In this case, the number of data points was increased till there was negligible difference between successive predicted values. Figure 7 shows the results obtained. Step 1 refers to predicted values for a single unknown and step 2 when both were taken as unknown. Clearly, the process converges to essentially unique values, with the two unknown cases taking more data points. In all these studies, no effort was made to optimize the location of the temperature sensor locations. Simply additional points were taken to reduce the error [19].

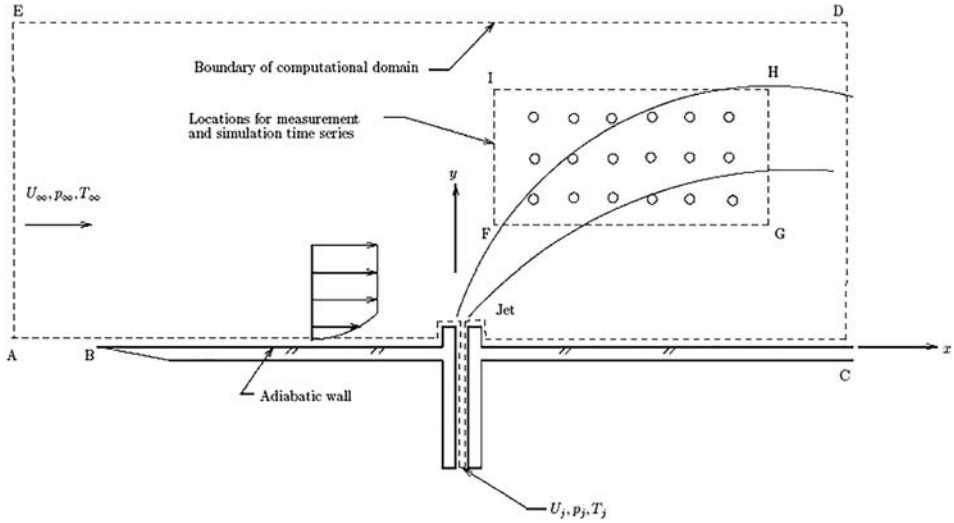

Fig. 5 Two-dimensional buoyant jet in a crossflow, along with locations for measurement and simulation to predict discharge conditions

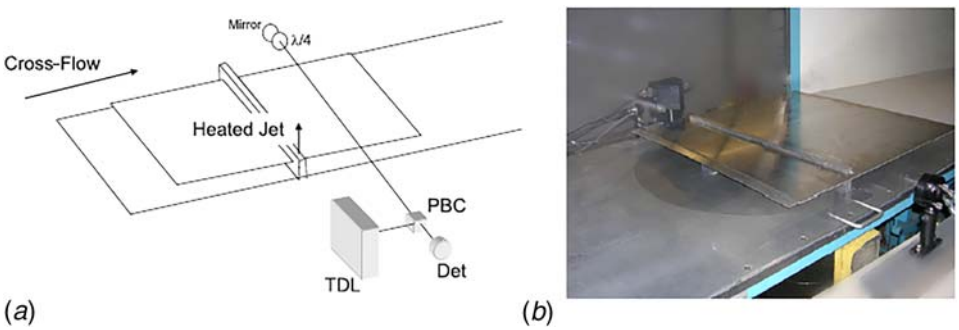

Fig. 6 Experimental arrangement for generating a two-dimensional buoyant jet in a free stream flow

Wall Plume and Jet Flows. A predictor–corrector method was developed to solve the inverse convection problem of a plume or jet in a cross-flow by Vanderveer and Jaluria [20,21]. The problem is similar to the one discussed in the Jets in Cross Flow section, though the solution methodology and optimization were quite different. Thus, the inverse problem involves the prediction of the strength and location of the heat source by employing a few selected data points downstream. This is accomplished with the help of numerical simulations of the region at differing source strengths, and thus, obtaining inverse interpolation functions.

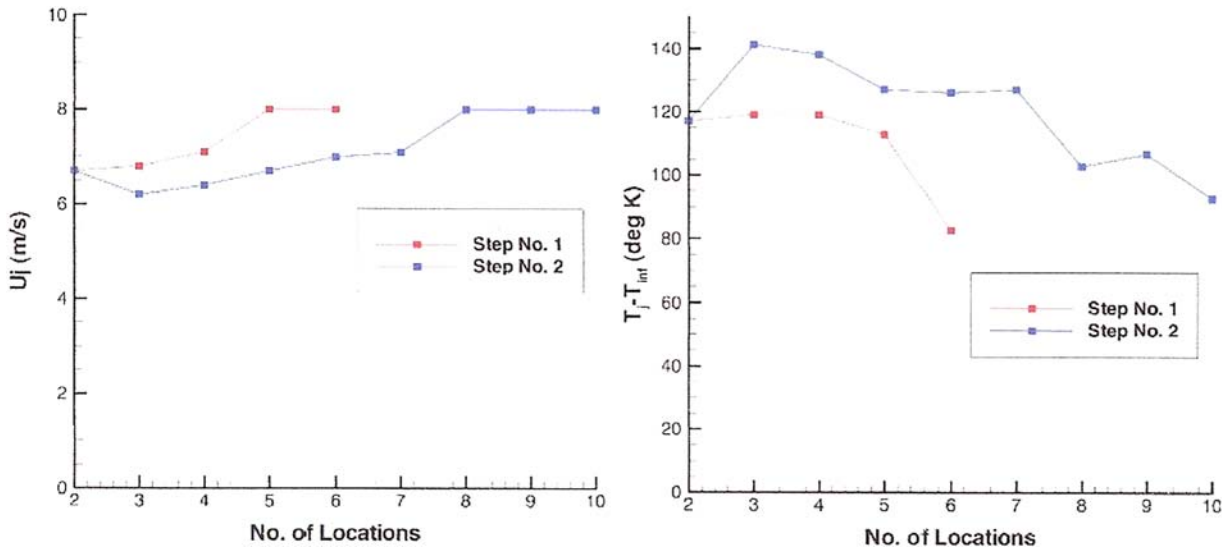

Fig. 7 Results from applying the inverse solution methodology to the flow circumstance of Fig. 5

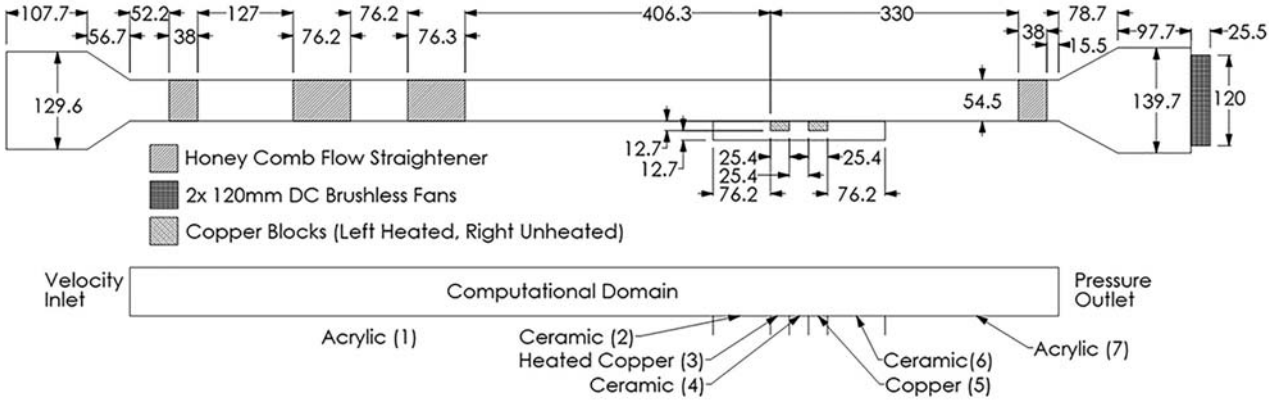

Fig. 8 Experimental arrangement and the computational domain for heat sources in a channel flow

Figure 8 shows a sketch of the experimental system and of the computational domain. The numerical results for the direct problem, in terms of isotherms and temperature profiles, are shown in Fig. 9. The results are also validated by comparisons with experiments.

On the basis of these results, interpolation functions are developed. These functions are employed in the predictor step to determine the source strength. Then, these interpolation functions are used, with adjustments based on the predictor, to determine the source location. The error is reduced by using a genetic algorithm optimization. Finally, experimental data are used to determine the strength and location of the source. Optimization of the location of the data points is used to minimize the number of samples needed for accurate predictions. The predictor-corrector method is shown to result in fairly unique solution of the inverse problem. The solution error is found to be less than a few percent. Figure 10 shows the region of uncertainty as it shrinks to a fairly narrow region through optimization of the locations where data are obtained. A comparison between predicted and actual source temperatures is also shown.

Figure 11 shows the error in predicting the source strength for a few random cases. It is seen that the error is sharply reduced by optimizing the locations where the data are taken. In general, points are needed with both vertical and horizontal separation to accurately determine the strength and location of the source. The error for several selected cases, as well as comparison between predicted and actual values, is shown in Fig. 12. Again, it is seen that the error is small, and a good agreement between actual and predicted values is obtained at optimized data collection.

Natural Convection Flows on a Vertical Surface. Wall plumes generated by a finite heat source on a vertical adiabatic surface are considered. This problem is of interest in wall fires and electronic systems with electronic components located on a

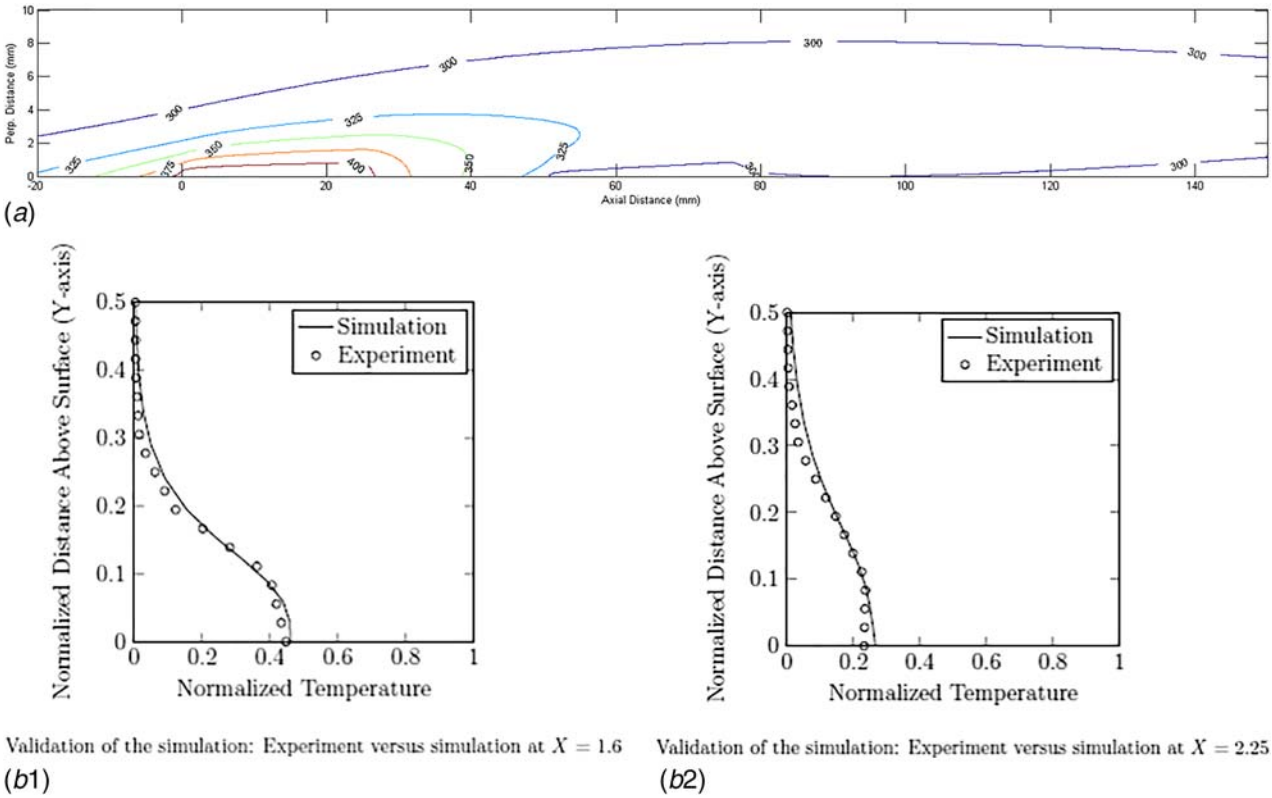

Fig. 9 Forward solution: (*a*) isotherms due to a finite-sized heat source in channel flow and (*b*) comparisons between simulation and experimental results on temperature profiles

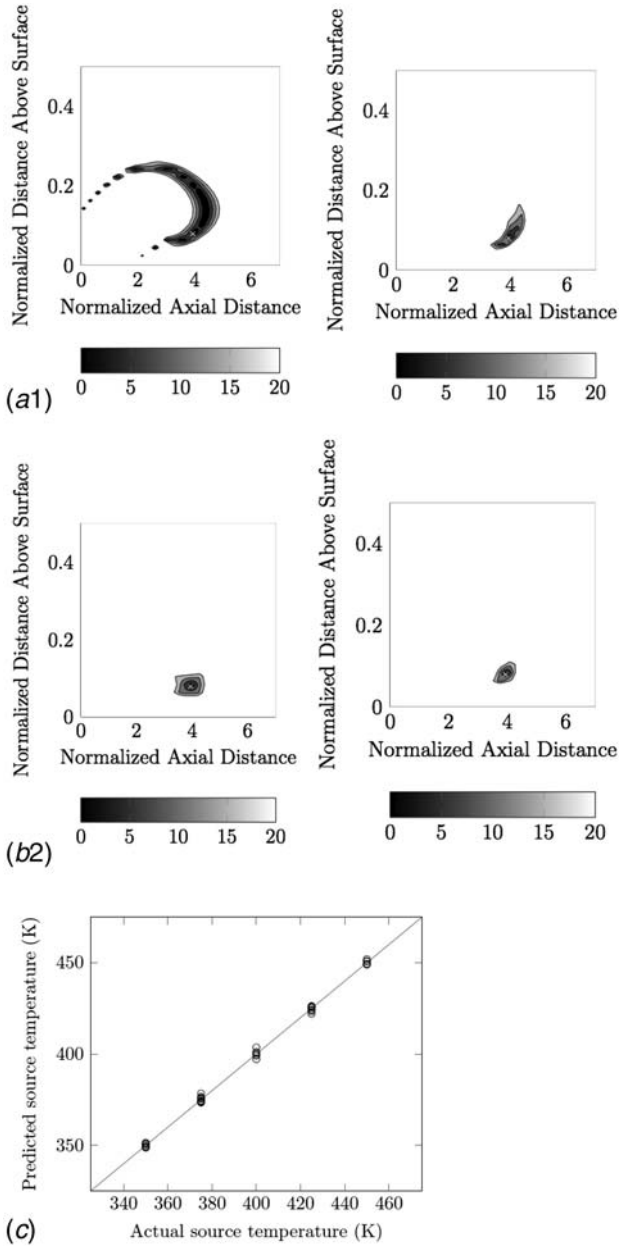

Fig. 10 (*a*, *b*) Narrowing of the region of uncertainty by optimizing the data locations and (*c*) actual versus predicted source temperature

wall. The heat input generates a plume adjacent to the wall. This plume is investigated in detail for both steady and transient cases to develop methodologies to solve the inverse problem of determining the source location and strength, using data taken downstream of the source. Figure 13(*a*) shows the geometry and coordinate system for this problem. The plate is taken as adiabatic except for the finite region where a uniform heat flux or isothermal conditions are imposed. This heated region represents a heat source such as an electronic component, a fire, or heat input in materials processing. Radiation effects are neglected [22]. Other similar studies have also been carried out [23–25]. Figure 13(*b*) shows a comparison between the results for an isothermal plate compared with results in the literature to validate the computational model [26].

The governing equations for this problem, after applying the Boussinesq approximations, the stream function, and vorticity formulation and nondimensionalizion, are given by the following:

$$\frac{D\omega}{Dt} = \mathrm{Pr}\cdot\nabla^2\omega + \mathrm{Gr}\,\mathrm{Pr}^2\frac{\partial T}{\partial y} \tag{6}$$

$$\frac{DT}{Dt} = \mathrm{Pr}\cdot\nabla^2 T \tag{7}$$

$$\nabla^2\psi = \bar{\omega} \tag{8}$$

where ω is the vorticity, ψ is the stream function, $\mathrm{Gr} = g\beta\Delta TL^3/\nu^2$ is the Grashof number D/Dt is the particle derivative, and $\mathrm{Pr} = \nu/\alpha$ is the Prandtl number. This is the forward or direct problem which results in velocity and temperature fields across the domain under given initial and boundary conditions. In this problem, Gr and l represent source strength and location, respectively.

First, the equations are solved to obtain the downstream temperatures as functions of the source strength, given in terms of the Rayleigh number Ra, and the location, given in terms of dimensionless distance l. Figure 14 shows some of these typical results. The variation of the wall temperatures at three downstream locations, as indicated in the figure, with the source location and strength is shown. These results are then used to obtain interpolation functions. Obviously, a wide variety of functions, such as polynomials, can be used to represent these results. The function that was found to represent the results quite closely was the following [27]:

$$T = a_1 Gr^{a_2}\cdot\ \exp\left[a_3\mathrm{Gr}^{a_4}\cdot l^{a_5}\right] \tag{9}$$

where a_1–a_5 are coefficients calculated at any point using nonlinear regression methods, Gr is the Grashof number, and l is the distance of the midlength of the finite source to the bottom of the plate. In order to find these coefficients, the results obtained by the forward solution are used.

After determining the coefficients of Eq. (9) for all possible locations, if the temperature at any given two points are known, a system of equations can be solved to determine Gr and l. The study tries to find the optimal pair of locations to put sensors in order to minimize the error in strength and location estimation. Particle swarm optimization (PSO) algorithm was selected to perform the optimization due to its simplicity and convergence speed [28]. PSO is a metaheuristic search-based method that was inspired by the behavior of a flock of birds or a school of fish searching for food [29]. In order to solve a problem, an initial and usually random set of candidate solutions, or in the case of this algorithm particles, is selected. These particles are then moved around in the search-space under the influence of their own personal best position as well as the swarm's best position. This way those particles that are on the better track can guide the rest of the swarm to the best position in the search-space. In order to find the best pair of points that yield the lowest error, PSO search algorithm is used with the objective function

$$\text{objective function} = w_1\left|\frac{\mathrm{Ra}_{\mathrm{est}} - \mathrm{Ra}}{\mathrm{Ra}}\right| + w_2\left|\frac{x_{\mathrm{est}} - x}{x}\right| \tag{10}$$

where w_1 and w_2 are weighting factors and subscript est indicates estimated values. Here, Ra indicates the strength and x the location of the source. PSO would find the pair that would result in the least objective function value. This iterative process continues until the accuracy criterion of the problem is met or a certain number of iterations have passed. A group of 16 data cases were chosen to train the PSO algorithm. The other group of data cases is referred to as testing data set. It should be noted that these coefficients are different for uniform heat flux sources.

The optimization process yields two points where the sensors may be placed for optimum results. The system of equations based on their respective relations is solved to obtain solution to the inverse problem. Figure 15 shows these two optimal locations and the resulting errors from this inverse calculation for a number

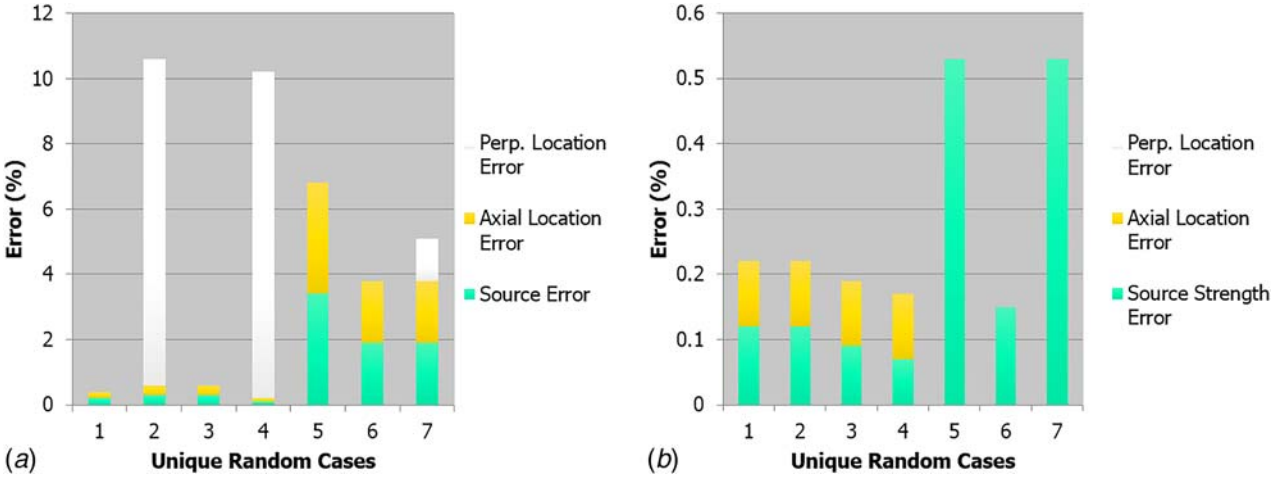

Fig. 11 Errors in the inverse solution using arbitrarily distributed data points and optimized distribution or shape

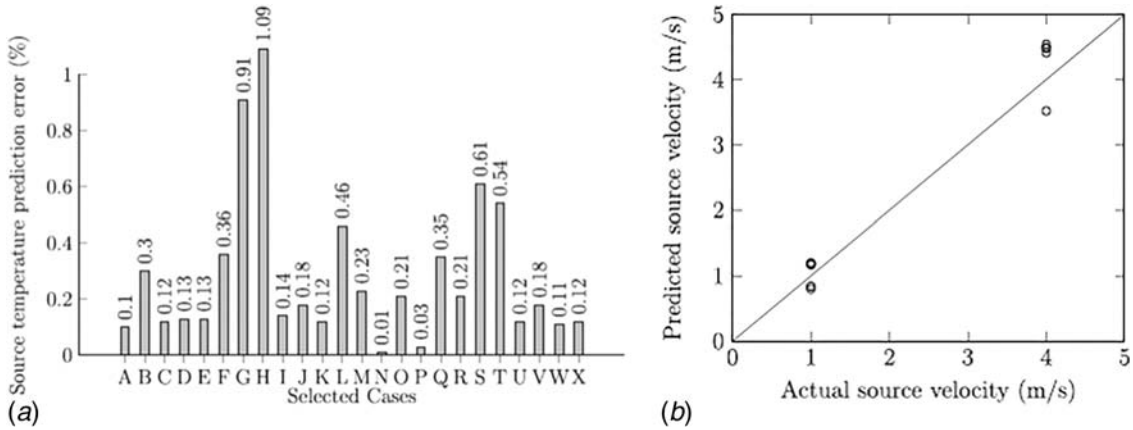

Fig. 12 Errors in the prediction of source temperature and velocity in a buoyant jet in crossflow

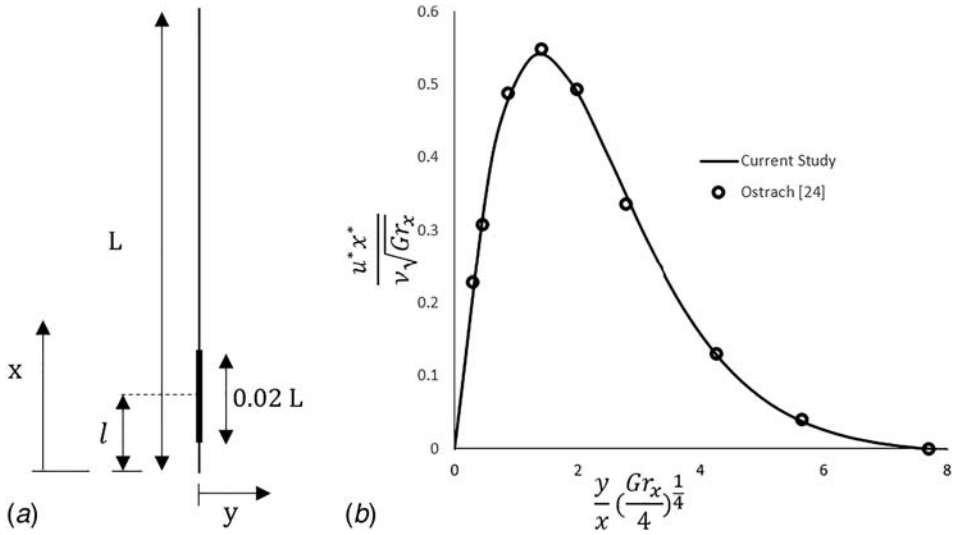

Fig. 13 (*a*) Geometry and coordinate system for a wall plume and (*b*) comparison of numerical results for natural convection boundary layer flow on an isothermal vertical surface with those in the literature

of cases for an isothermal source. The error in location is found to be greater than that in the source strength, as seen in other cases as well. Figure 16 shows the results for the uniform heat flux condition at the source. Again, the results from the inverse solution are fairly close to the actual location and strength of the heat source. The transient results can also be used effectively to determine the source location and heat input. This approach is presently being pursued.

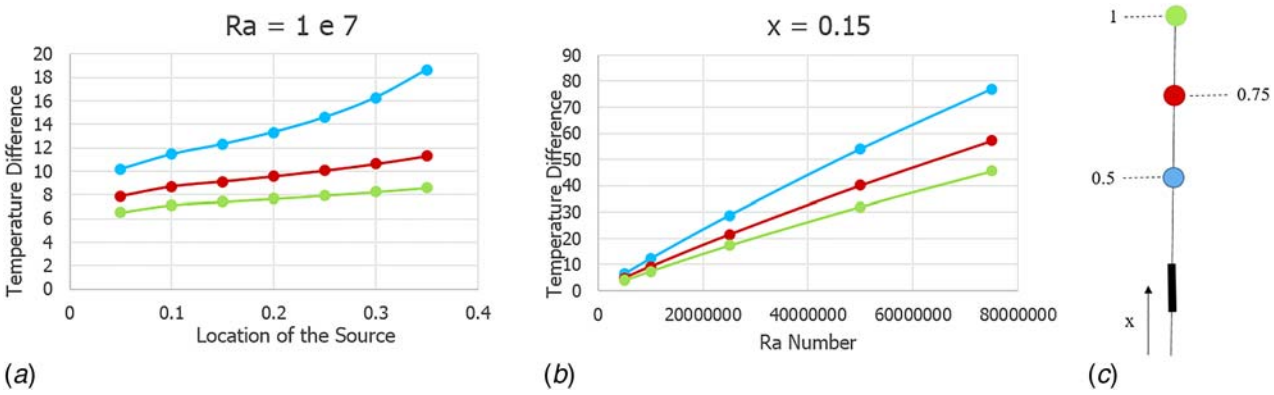

Fig. 14 Temperature variation with respect to source location (left) and Ra number (right)

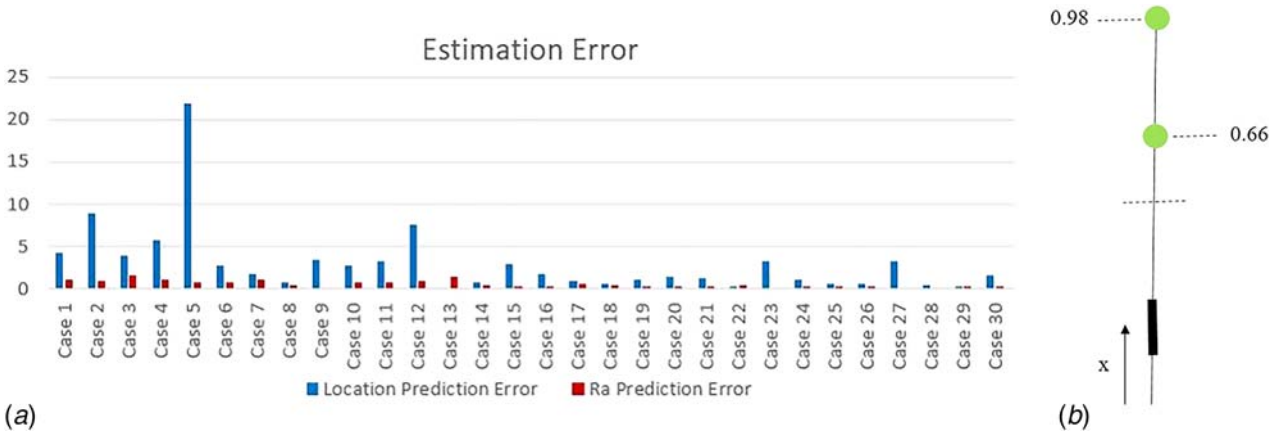

Fig. 15 Estimation error diagram for location and source strength, given in terms of the Rayleigh number, Ra, for an isothermal heat source

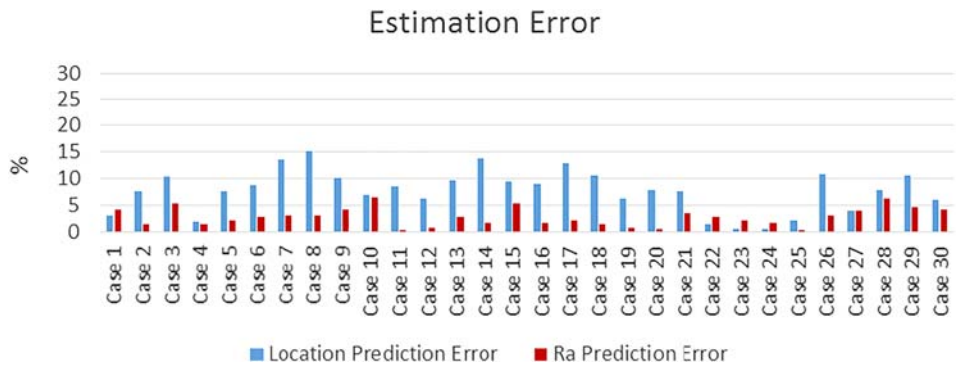

Fig. 16 Estimation error diagram for location and Ra number for a uniform heat flux input at the source

4 Conclusions

The solution of inverse problems in which the desired outcome or result is known, but the conditions that lead to this result are not known, frequently arise in thermal processes and systems. This paper discusses problems where an inverse solution is needed to obtain the conditions to achieve a desired result or to complete a given problem in which the boundary conditions are not known. The results from an inverse solution are generally not unique and the optimization is needed to obtain a narrow region of uncertainty. Different strategies to obtain the conditions that lead to a desired result are given. The forward or direct solutions are used to generate results that are used to obtain appropriate interpolation functions. These functions are used to predict the unknown parameters and conditions. These predictions are corrected to increase the accuracy with which the conditions are determined. Optimization is used to reduce the uncertainty and obtain essentially unique solutions for different circumstances. The error of the method can be checked against known conditions to see if it is acceptable for the given problem. It is found that the locations at which data are taken to determine a particular input condition, such as temperature, inlet velocity, or heat input, can be optimized to minimize the number of data points or sensor measurement needed for desired accuracy. Several examples are given to illustrate the use of these methods.

References

[1] Li, T., ed., 1985, *Optical Fiber Communications, Vol. 1: Fiber Fabrication*, Academic Press, New York.

[2] Jaluria, Y., 2017, "Thermal Transport in the Manufacture of Optical Fibers," Ann. Rev. Heat Transfer, **20**, pp. 193–239.

[3] Ozisik, M. N., 2000, *Inverse Heat Transfer: Fundamentals and Applications*, Taylor & Francis, Philadelphia, PA.
[4] Orlande, H. R. B., Fudym, O., Maillet, D., and Cotta, R. M., 2011, *Thermal Measurements and Inverse Techniques*, Taylor and Francis Group, CRC Press, Boca Raton, FL.
[5] Orlande, H. R. B., 2012, "Inverse Problems in Heat Transfer: New Trends on Solution Methodologies and Applications," ASME J. Heat Transfer, **134**(3), p. 031011.
[6] Ghosh, A., and Mallik, A. K., 1986, *Manufacturing Science*, Ellis Horwood, Chichester, UK.
[7] Jaluria, Y., 1984, "Numerical Study of the Thermal Processes in a Furnace," Numer. Heat Transfer, **7**(2), pp. 211–224.
[8] Jarny, Y., Ozisik, M. N., and Bardon, J. P., 1991, "A General Optimization Method Using Adjoint Equation for Solving Multidimensional Inverse Heat Conduction," Int. J. Heat Mass Transfer, **34**(11), pp. 2911–2919.
[9] Prud'homme, M., and Nguyen, T. H., 2001, "Solution of Inverse Free Convection Problems by Conjugate Gradient Method: Effects of Rayleigh Number," Int. J. Heat Mass Transfer, **44**, pp. 2011–2027.
[10] Burmeister, L. C., 1993, *Convective Heat Transfer*, 2nd ed., Wiley Interscience, New York.
[11] Stikker, U. O., 1970, "Numerical Simulation of the Coil Annealing Process," Math. Models Metall. Proc. Dev., Iron Steel Inst., Spec. Rep., **123**, pp. 104–113.
[12] Harvey, G. F., 1977, "Mathematical Simulation of Tight Coil Annealing," J. Australas. Inst. Met., **22**, pp. 28–37.
[13] Jaluria, Y., 2008, *Design and Optimization of Thermal Systems*, 2nd ed., CRC Press, Boca Raton, FL.
[14] Cheng, X., and Jaluria, Y., 2005, "Effect of Furnace Thermal Configuration on Optical Fiber Heating and Drawing," Numer. Heat Transfer, **48**(6), pp. 507–528.
[15] Paek, U. C., 1999, "Free Drawing and Polymer Coating of Silica Glass Optical Fibers," ASME J. Heat Transfer, **121**(4), pp. 775–788.
[16] Izawa, T., and Sudo, S., 1987, *Optical Fibers: Materials and Fabrication*, KTK Scientific Publishers, Tokyo, Japan.
[17] Issa, J., Yin, Z., Polymeropoulos, C. E., and Jaluria, Y., 1996, "Temperature Distribution in an Optical Fiber Draw Tower Furnace," J. Mater. Process. Manuf. Sci., **4**(3), pp. 221–232.
[18] Ma, Q., Luo, Y., Rossmann, T., Knight, D., and Jaluria, Y., 2006, "Diode Laser Measurements for DDDAS: Flow Field Reconstruction Using Dynamic Experimental and Numerical Data," AIAA Paper No. 2006-2974.
[19] Knight, D., Ma, Q., Rossman, T., and Jaluria, Y., 2007, "Evaluation of Fluid-Thermal Systems by Dynamic Data Driven Application Systems—Part II," International Conference on Computational Science, Reading, UK, May 28–31, pp. 1189–1196.
[20] Vanderveer, J. R., and Jaluria, Y., 2013, "Solution of an Inverse Convection Problem by a Predictor–Corrector Approach," Int. J. Heat Mass Transfer, **65**, pp. 123–130.
[21] Vanderveer, J. R., and Jaluria, Y., 2015, "Optimization of an Inverse Convection Solution Strategy," Int. J. Heat Mass Transfer, **73**, pp. 664–670.
[22] Mossi, A., Vielmo, H., Franca, F., and Howell, J., 2008, "Inverse Design Involving Combined Radiative and Turbulent Convective Heat Transfer," Int. J. Heat Mass Transfer, **51**(11–12), pp. 3217–3226.
[23] Hong, Y. K., Baek, S. W., and Kim, M. Y., 2010, "Inverse Natural Convection Problem With Radiation in Rectangular Enclosure," Numer. Heat Transfer, **57**(5), pp. 315–330.
[24] Park, H., and Chung, O., 1999, "An Inverse Natural Convection Problem of Estimating the Strength of a Heat Source," Int. J. Heat Mass Transfer, **42**(23), pp. 4259–4273.
[25] Ghosh, S., Pratihar, D., Maiti, B., and Das, P., 2011, "Inverse Estimation of Location of Internal Heat Source in Conduction," Inverse Probl. Sci. Eng., **19**(3), pp. 337–361.
[26] Ostrach, S., 1953, "An Analysis of Laminar Free-Convection Flow and Heat Transfer About a Flat Plate Parallel to the Direction of the Generating Body Force," NASA, Washington, DC, Report No. NACA-TR-1111.
[27] Tabrizi, A. B., and Jaluria, Y., 2018, "An Optimization Strategy for the Inverse Solution of a Convection Heat Transfer Problem," Int. J. Heat Mass Transfer, **124**, pp. 1147–1155.
[28] Poli, R., 2008, "Analysis of the Publications on the Applications of Particle Swarm Optimization," J. Artif. Evol. Appl., **2008**, pp. 1–10.
[29] Kennedy, J., 1997, "The Particle Swarm: Social Adaptation of Knowledge," IEEE International Conference on Evolutionary Computation, Indianapolis, IN, Apr. 13–16, pp. 303–308.